Impulse noise recuperation from grayscale and medical images using supervised curve fitting linear regression and mean filter

Shiju Thomas[1,2], Addapalli Krishna[1]

[1]Department of Computer Science and Engineering, School of Engineering and Technology, Christ University, Karnataka, India
[2]Department of Computer Science, Rajagiri College of Social Sciences, Mahatma Gandhi University, Kerala, India

Article Info

ABSTRACT

Acquisition of images from electronic devices or Transmission of the image through any medium will cause an additional commotion. This study aims to investigate a framework for eliminating impulse noise from grayscale and medical images by utilizing linear regression and a mean filter. Linear regression is a supervised machine learning algorithm that computes the value of a dependent variable based on an independent variable. The value of the recuperating pixel is measured using a curve-fitting, direction-based linear regression approach or applying a mean filter to the noise-free pixels. The efficiency of the proposed technique experiments with benchmark test images and the images of the USC-SIPI and TESTIMAGES data sets. Peak signal-to-noise ratio (PSNR) and structural similarity index metrics (SSIM) are determined to prove the performance of the proposed method. The results, when compared with the seven recent state-of-the-art techniques, show the superiority of the proposed method in terms of visual quality and accuracy. The proposed model achieves an average PSNR value of 65.21dB and an SSIM value of 0.999 for the reconstruction of medical images, proving its accuracy and efficiency. The impulse noise restoration process helps the radiologist get a clear visual clarity of the medical image for diagnosis purposes.

Corresponding Author:

Shiju Thomas
Department of Computer Science and Engineering, School of Engineering and Technology
Christ University
Karnataka, India
Email: shijuthomascochin@gmail.com

1. INTRODUCTION

Signal processing is a branch of electronic engineering that employs a variety of processes to analyze and modify images, allowing for the most accurate scientific inferences. Digital Image Processing algorithms are applied to enhance or reinforce a digital image. The recovery or convalescence of images by removing the noise contained in them is one of the most challenging areas of image processing. Pre-processing ensures that the unwanted information is isolated from the input data. Image restoration has a vital role within the medical imaging field. In medical image processing, the collected medical image data is passed through numerous channels or mediums to destinations in several formats, like digital imaging and communication in medicine (DICOM). This study eliminates impulse noise from grayscale images using the rectilinear regression followed by the linear mean filter.

Noise recuperation using linear and nonlinear filters has been the subject of extensive research. A median filter is a nonlinear filter implemented in an adaptive weighted median filter or a switching median filter. On the other hand, the mean is a linear filter implemented for the same by incorporating an iterative

mean filter or weighted mean filter. Recent studies show that the combination of median and mean filters is applied to the recuperation process. A modified cascade channel [1] is used to eliminate high-thickness salt-and-pepper noise is implemented, which makes use of an aggregate trimmer median filter (TMF) and a decision-based median filter (DMF). Recent studies exploit machine learning techniques [2], convolutional neural network (CNN) models [3] and deep learning techniques [4] using the divide and conquer approach for image denoising. In contrast to customary methodologies that learn clean images from uproarious images, the model [5] uses residual learning, which takes in commotion from noisy images and afterwards deducts it from noisy images in order to get perfect pictures. Garg [6] implements an adaptive weighted minimal and maximum median filter, in which the window dimension is increased following the window's corruption-free pixel status, and the noisy pixel's value is determined using the weighted median filter. Two novel median filter algorithms are introduced in [7], [8] for the recuperation of noise from the grey levels, utilising the rank order-based adaptive median filter and the impulse size-based adaptive median filter, respectively. A two-stage iterative filter [9] and a non-linear non-local adaptive switching median filter [10] are applied for the recuperation process. The non-local mode is most effective when the window has many noisy pixels. A hybrid strategy for restoration was applied [11], using the highest frequency non-corrupted pixel in the operative region and an applied median filter. A modified pixel median filter for the recuperation process is mastered in [12]. The study performed in [13] utilises the frequency of the non-corrupted pixels to compute the grey value of the noisy pixels within the region. An adaptive fuzzy detector [14], is applied to detect the salt and pepper noise and a weighted mean filter to restore the same. A fuzzy mathematical morphological open-close filter [15] uses only uncorrupted pixels for computing the pixel value for eliminating salt and pepper noise. A sparse recuperation model for impulse noise is proposed in [16].

Image noise restoration has a wide range of real-life applications. Medical imaging is one of the relevant areas of image processing in medicine. The medical images generated from various electronic devices include noises. For interpretation purposes, preprocessing techniques like visualization, smoothing, edge detection, and restoration are applied to the input image. A fuzzy rule-based system for restoration of random impulse noise is experimented with in [17]. An S-curve logistic regression technique is mastered in [18] for the prediction of diabetes. The linear regression technique [19], [20] is applied for the automatic prediction of missing values. A threshold-based technique is employed to reduce noise, and a locally adaptive threshold-based edge preservation denoising scheme is used [21]. Digital image transformation [22] techniques are applied to remove noise from medical images. A hybrid technique of a modified median filter and a Wiener filter [23] was used to restore the noise from images using morphological image processing operations. A nonlinear fuzzy filter [24] using a computational intelligence algorithm is applied to medical images to remove impulse noise. A type-2 fuzzy kernel for eliminating impulse noise from the grayscale image has been proposed in [25], which uses the combination of mean and variance for the restoration process. A fuzzy logic technique [26], a direction-weighted mean filter [27], and a Quaternion two-stage filter [28] are applied to eliminate noise from medical images.

2.   RESEARCH METHOD

The block diagram for the proposed scheme is available in Figure 1. The experiment consists of two major sections. First, the restoration value for the corrupted pixel is computed by applying the linear regression method to each direction. The value obtained in the regression method is given to the mean filter in the second stage for determining the recuperating value. If there are no valid directions, then the recuperating value is computed using the uncorrupted pixels in the window. A generalised flowchart for the proposed model is available in Figure 2.
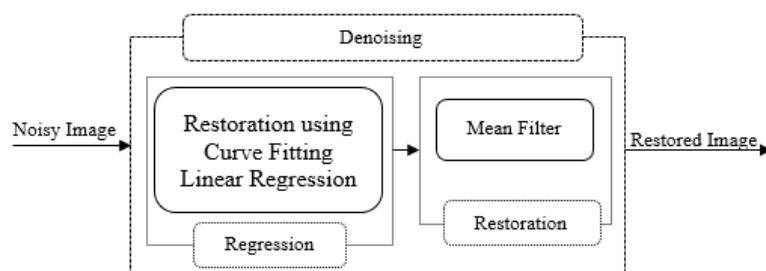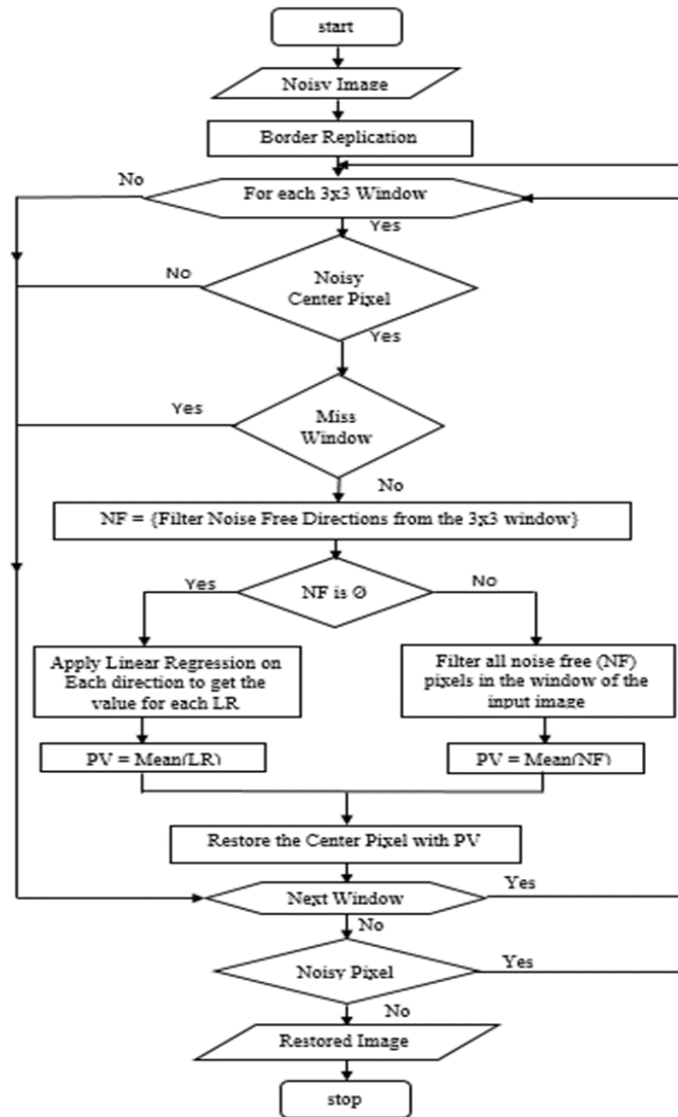
Figure 1. Block diagram

Figure 2. Flowchart for the proposed model

The proposed algorithm for noise restoration has two parts: noise detection and noise restoration. Noise restoration algorithm is depticted in Figure 3. The algorithm reads a noisy grayscale or a dicom image and applies a border replication algorithm to enhance the image, to perform operations based on a 3x3 structuring element. For each noisy window detected, it uses the Restore-Window algorithm, explained in Algorithm 2 as shown in Figure 4, to compute the restoration value for the corrupted pixel.

2.1. Hit and miss window

The restore window algorithm operates on the noisy window to identify all pairs of noise-free pixels in all possible directions. If there are no noise-free directions, then a mean filter is applied to the noise-free pixels on the window to compute the pixel value for the noisy centre pixel. Otherwise, for each noise-free direction, all the pixel values of the noise-free pixels in the window between the two values of the selected noise-free direction are used for computing the restoration value using curve fitting linear regression. The process is repeated for all noise-free directions, and a mean filter is applied to the computed pixel values to get the restoration value. It depends on the nature of the pixels and the origin of the operating region. The windows are classified into two categories: miss-window and hit-window. The window in which no recuperation process is performed is called the miss-window. The two scenarios leading to miss-window are visualized in Figure 5. Figure 5(a) explains the first case in which the origin of the kernel is an uncorrupted pixel and no recuperation process is performed. Figure 5(b) depicts the second scenario in which every pixel is noisy, including the center pixel, and thus no operation is performed.

Algorithm 1 Noise Restoration

Data: NI = A Noisy grayscale or DICOM Image
Result: RI = Restored Image
$W \leftarrow Width(NI)$ ▷ Width of the Image
$H \leftarrow Height(NI)$ ▷ Height of the Image
$II \leftarrow BorderReplication(NI)$ ▷ EnhancedInput Image II
$RI \leftarrow II$ ▷ Output Image Initialization
for *each, noisypixel* ∈ *II* **do**
  $window \leftarrow Window(\text{noisypixel})$
  if *window is hitwindow* **then**
    $pv \leftarrow Restore - Window(window)$ ▷ Algorithm 2
    $RI_{ij} \leftarrow pv$
  end
end

Figure 3. Noise restoration algorithm

Algorithm 2 Restore Window

Data: IW = A 3x3 window with noisy origin and having at least one corrupted pixels
Result: pv = Restored pixel value
$DNF \leftarrow Filter - Noise - Free - Directions(IW)$ ▷ Filter all pair of pixels in the four directions having
  noise free pixel pair
$NF \leftarrow All - Noise - Free - Pixels(IW)$
if DNF *is* ∅ **then**
  $pv \leftarrow Mean(NF)$ ▷ *No Direction - Apply Mean Filter*
else
  $LR \leftarrow ∅$
  for *each, DirectionD* ∈ *IW* **do**
    $min \leftarrow Minimum - Pixel(D)$
    $max \leftarrow Maximum - Pixel(D)$
    $MLR \leftarrow Filter - Pixels - Between(min,max)$
    $LR \leftarrow Union(LR, Mean(MLR))$ ▷ *Direction Based Linear Regression*
  end
  $pv \leftarrow Mean(LR)$ ▷ *Restoration Value Computation from the regression values*
end

Figure 4. Restore window algorithm

255	0	255
0	100	0
255	0	255

255	0	255
0	255	0
255	0	255

(a)   (b)

Figure 5. Miss window scenario, (a) noise free center pixel and (b) all pixels are noisy including origin

2.2. Direction based supervised linear regression

The window in which the origin pixel is a noisy one with a few noise-free pixels available is called the hit window. Based on the number of noise-free pixel directions in the hit window, the recuperation process takes place in two approaches. They are direction-based linear regression followed by a mean filter and a non-direction-based mean filter. In a 3x3 window, there are four directions concerning the origin pixel, where each edge consists of two pixels on the sides, with the noisy pixel in the center. Direction-based linear regression is applied only if both the pixels on the edges are noise-free. All the uncorrupted pixel values are stored in an array and are given to the linear regression function to predict the best match for substituting the corrupted pixel value. The different direction-based linear regression scenarios are classified into tetra, tri, bi, and mono-directional. The window consists of only noisy pixels at the origin of the kernel is called tretra direction window, shown in Figure 6. All four directions centred on the kernel pixel can be used for calculating the recuperation value for the centre pixel as shown in Figure 6(a), and Figure 6(b) shows it in shaded color.
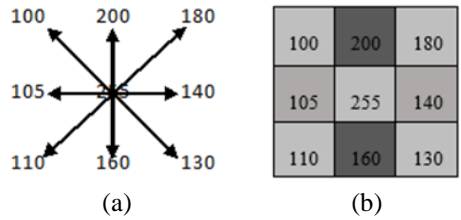
(a)   (b)

Figure 6. Tetra direction window, (a) Noisy center pixel with four direction edges and (b) pixel directions in different shaded color

In each of the four directional edges, the linear regression algorithm selects the four most suitable values from the list of noise-free pixels. The process is applied only if both the pixels in the directions are noise-free.

D1-{110, LR1, 180}
D2-{105, LR2, 140}
D3-{100, LR3, 130}
D4-{200, LR4, 160}

To calculate the value of LR1, the minimum value is 110 and the maximum value is 180. All non-corrupted pixel values between minimum and maximum value, including them are {110, 130,140,160,180}.

LR1 is the mean of these values.
LR1=(110 + 130 + 140 + 160 + 180)/5=144

Similarly, Other values are calculated as
LR2=(105 + 110 + 130 +140) / 4 = 121
LR3=(100 + 105 + 110 + 130) / 4 = 111
LR4=(160 + 180 + 200) / 3 = 180

Calculate the mean of the values obtained, and that will be the pixel value restored for the noisy pixel.
PV=(LR1 + LR 2 + LR 3 + LR 4) / 4
PV=(144 + 121 + 111 + 180) / 4
PV=139

The calculation procedure explained above is commonly applied to all hit windows having tri-direction, bi-direction, and mono-direction.

2.3. Non direction based linear mean filter operation

When there is no direction of noise-free pixels available with a pair of noise-free pixels, the proposed scheme computes the restoration value by applying a mean filter to all uncorrupted pixels in the operating region. Figure 7 demonstrates the scenario. The noise free pixels are {200, 135, 110, and 110}.

PV = (200 + 135 + 110 + 110) / 4
PV = 139

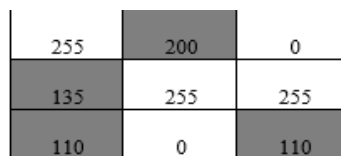The determined value 139 is used to restore the centre pixel.

Figure 7. Non-direction window

3. RESULTS AND DISCUSSION

Experiments with standard images from the literature, sample images from the USC-SIPI dataset, and 40 images from the TESTIMAGES dataset are used to assess the proposed system's effectiveness. The tool utilized for directing the investigation is MATLAB R2016a. The conventional visual quality estimate measures [29] peak signal to noise ratio (PSNR), structural similarity index (SSIM), and Histogram are utilised to assess the efficacy of the results produced. The accuracy of the proposed scheme is shown by a histogram plot comparison of the original and restored images. The suggested approach restores noise density from 10% to 90% in DICOM images with exceptional results.

3.1. Peak signal to noise ratio (PSNR)

PSNR is used to evaluate the reproduction quality of images. The peak signal-to-noise ratio is a standard metric for measuring the fidelity between the source and recuperated image. The PSNR ratio is determined using (1).

$$PSNR\ (in\ dB) = \frac{255^2}{\frac{1}{W\,X\,H}\ \sum_{p=1}^{W}\sum_{q=1}^{H}(SI(p,q)-\ RI(p,q))^2} \tag{1}$$

Where W and H are the image width and height, and SI[p, q], RI[p, q] is the pth row, q^{th} column pixel in the source and recuperated image, respectively. The prospective framework has experimented with standard test images from literature and sample images from the USC-SIPI dataset. The results computed for the PSNR values are shown in Table 1. Figure 8 shows the corrupted image and the respective recuperated image for the impulse noise density of 30%, 50%, 70%, and 90%, respectively, for the images Pepper, Baboon, and USC-SIPI-1 of size 512x512. Figure 9 shows the histogram comparison of Baboon, Family, and USC-SIPI-1 recuperated images with 90% impulse noise and the source image.

Table 1. The obtained PSNR values for standard test images and images from the USC-SIPI data set

| Image	10	20	30	40	50	60	70	80	90
Pepper	44.37	41.02	38.82	37.08	35.54	33.92	31.74	30.02	27.24
Gold hill	42.32	39.11	37.07	35.43	33.99	32.46	30.68	29.17	26.86
Girl	44.32	40.91	38.95	37.13	35.33	33.64	31.61	30.16	27.45
Family	44.07	40.82	38.49	36.61	34.78	33.12	30.76	29.21	26.40
Baboon	33.60	30.41	28.40	26.91	25.66	24.43	23.19	21.93	20.51
Usc-Sipi-1	42.62	39.31	36.98	35.26	33.40	31.69	30.02	28.29	25.52
Usc-Sipi-2	41.18	37.87	35.77	34.06	32.53	31.00	29.51	27.90	25.45
Usc-Sipi-3	42.34	39.19	37.09	35.38	33.83	32.35	30.83	29.27	27.27
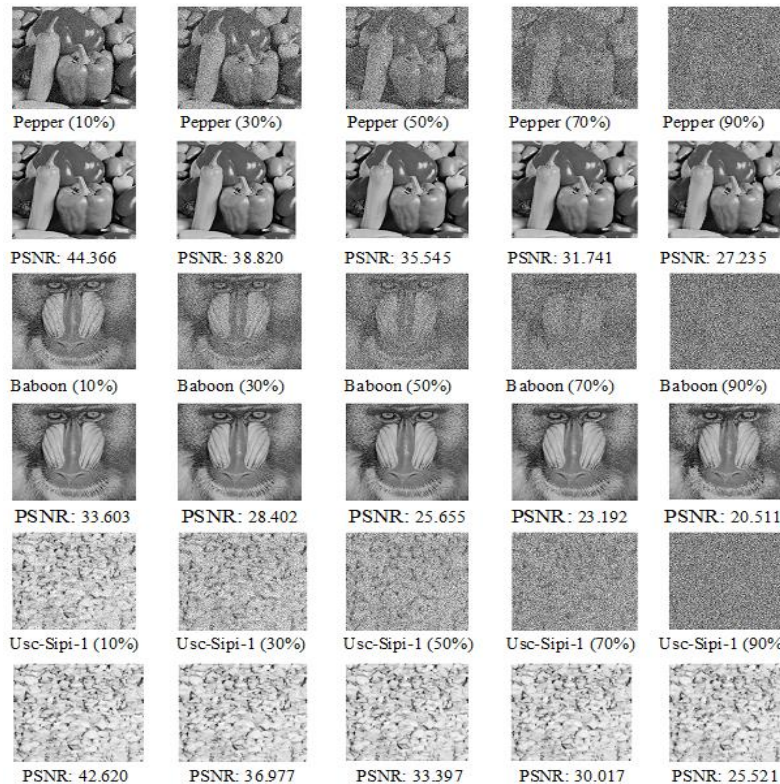
Figure 8. The noisy Pepper, Baboon, and USC-SIPI-1 images with 10%, 30%, 50%, 70%, and 90% impulse noise, and the restored images
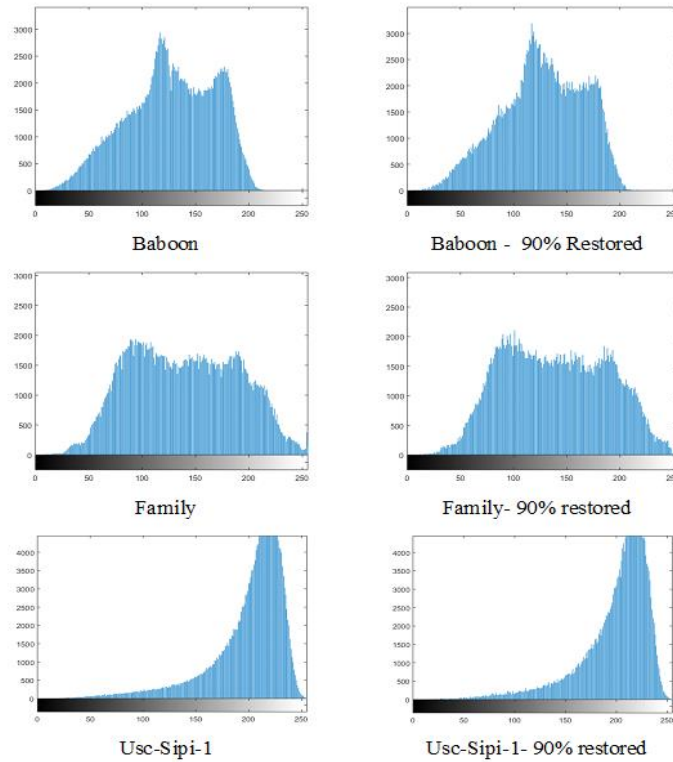
Figure 9. Histogram comparison of the source image with a restored image having 90% impulse noise

3.2. Structure similarity index metric

The structural similarity index metric measures the structural change in the image, which results in the degradation of the visual quality of an image with respect to the source image. The SSIM value is determined using (2), which takes the source (SI) and recuperated (RI) image as the input. Upon evaluation, the computed high SSIM value implies a close similarity between the source and the recuperated image. Table 2 shows the SSIM results for the ten standard test images chosen from the literature.

$$SSIM(SI, RI) = \frac{(2\mu_{SI}\mu_{RI}+C_1)+(2\sigma_{SIRI}+C_2)}{(\mu_{SI}^2+\mu_{RI}^2+C_1)(\sigma_{SI}^2+\sigma_{RI}^2+C_2)} \qquad (2)$$

Table 2. The obtained SSIM values for standard test images and images from the USC-SIPI data set

Image	10	20	30	40	50	60	70	80	90
Pepper	0.993	0.985	0.977	0.967	0.955	0.939	0.914	0.880	0.828
Gold hill	0.989	0.977	0.963	0.947	0.926	0.900	0.859	0.811	0.723
Girl	0.994	0.987	0.979	0.968	0.954	0.934	0.903	0.869	0.788
Family	0.995	0.990	0.984	0.974	0.962	0.941	0.908	0.874	0.786
Baboon	0.977	0.950	0.919	0.883	0.841	0.790	0.726	0.641	0.516
Usc-Sipi-1	0.989	0.976	0.961	0.944	0.922	0.894	0.860	0.815	0.735
Usc-Sipi-2	0.986	0.970	0.951	0.929	0.903	0.869	0.826	0.768	0.665
Usc-Sipi-3	0.983	0.966	0.947	0.924	0.898	0.866	0.826	0.776	0.704

3.3. Experiment result on TESTIMAGES dataset

The proposed framework outperformed the majority of recent studies when tested with 40 images from the TESTIMAGES [30] data set. Figure 10 shows the comparison of the proposed method with 7 recent studies with a noise density of 80%. Figures 10(a) and (b) show the comparison of the PSNR and SSIM value of the proposed method with seven recent studies. The results obtained for PSNR and SSIM were compared with seven recent studies and found that the proposed framework outperforms all the others with noise density from low-density to high-density. Table 3 shows the results of forty images from the TESTIMAGES dataset with noise densities of 20%, 40%, 60%, and 80%, and the PSNR and SSIM values obtained after the recuperation process.

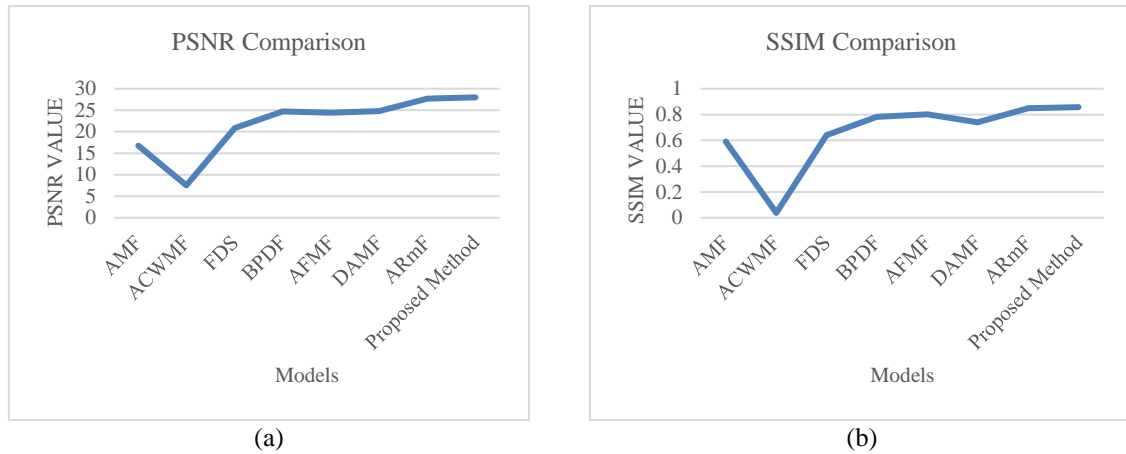(a)   (b)

Figure 10. Comparison of the proposed method with 7 recent studies with a noise density of 80% (a) PSNR value comparison and (b) SSIM value comparison

Table 3. Result analysis of 40 images from the TESTIMAGES dataset, with PSNR and SSIM values from the proposed approach compared to 7 recent studies

Algorithm	Criterion	20%	40%	60%	80%
AMF	psnr	25.9	22.68	20.57	16.74
	ssim	0.9502	0.9083	0.8401	0.5922
ACWMF	psnr	29.17	18.28	11.72	7.55
	ssim	0.9078	0.5013	0.1493	0.0384
FDS	psnr	32.37	30.37	25.78	20.88
	ssim	0.9587	0.9246	0.8244	0.6401
BPDF	psnr	32.15	29.49	27.78	24.72
	ssim	0.9595	0.9176	0.867	0.7828
AFMF	psnr	32.57	29.59	27.2	24.44
	ssim	0.9611	0.938	0.8938	0.8028
DAMF	psnr	34.14	30.3	27.63	24.8
	ssim	0.9113	0.8752	0.8244	0.7398
ARmF	psnr	39.4	35.3	31.701	27.72
	ssim	0.9844	0.9637	0.9268	0.8498
Proposed Method	psnr	39.2	35.35	31.711	27.99
	ssim	0.9836	0.9638	0.9269	0.8572

3.4. Image Denoising in Medical DICOM Images

In medical image processing, one of the standard formats for storing scanned images is called digital imaging and communications in medicine (DICOM). The primary reason for using this format is to transmit visual data through any communication channel. During transmission, the data may get corrupted by impulse noise. This impulse noise in the DICOM image is eliminated using curve fitting and linear regression. Figure 11 shows a sample DICOM image with noise restored. The high PSNR and SSIM values prove the efficacy of the proposed framework. From Table 4, it is evident that the SSIM value is 100% in most of the recuperation processes.

Table 4. The PSNR and SSIM values for the six dicom images restored from impulse noise 10% to 90%

| Image	Criterion	10	20	30	40	50	60	70	80	90	Average
dicom-1	psnr	77.61	73.96	72.19	70.42	68.41	66.32	64.50	61.31	57.62	68.04
	ssim	1.00	1.00	1.00	1.00	1.00	1.00	1.00	1.00	1.00	1.00
dicom-2	psnr	77.52	74.06	71.98	70.37	68.77	67.28	64.59	62.02	57.14	68.19
	ssim	1.00	1.00	1.00	1.00	1.00	1.00	1.00	1.00	1.00	1.00
dicom-3	psnr	78.91	75.88	74.03	72.21	70.48	68.84	66.72	64.11	59.78	70.11
	ssim	1.00	1.00	1.00	1.00	1.00	1.00	1.00	1.00	1.00	1.00
dicom-4	psnr	78.20	74.71	72.97	71.21	69.82	68.03	66.04	63.65	59.92	69.39
	ssim	1.00	1.00	1.00	1.00	1.00	1.00	1.00	1.00	1.00	1.00
dicom-5	psnr	76.80	73.45	71.40	69.98	68.35	66.53	64.56	62.35	58.88	68.03
	ssim	1.00	1.00	1.00	1.00	1.00	1.00	1.00	1.00	1.00	1.00
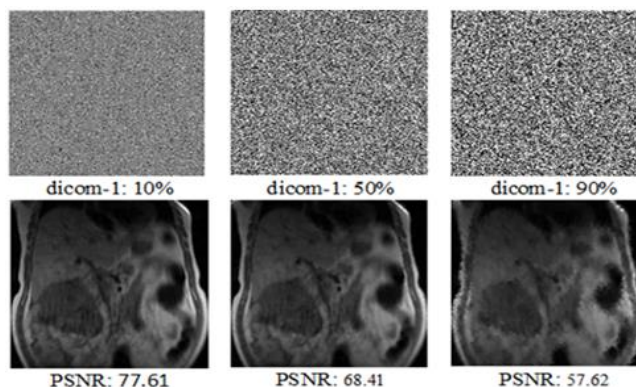
Figure 11. DICOM image noise restoration from noise densities of 10%, 50%, and 90%

4. CONCLUSION

In this study, a combined framework is mastered for the impulse noise recuperation of grayscale and DICOM medical images. The developed supervised technique combines the concepts of linear regression and linear mean filtering to create a hybrid framework for impulse noise recovery. The experimental result metric having high values for PSNR and SSIM proves the standard of the proposed framework. The scheme is also applied to remove the noise from medical DICOM images and which helps the radiologist to make inferences from the restored image. However, the proposed technique may be further advanced by incorporating deep learning techniques into the noise restoration process.

REFERENCES

[1] B. Karthik, T. K. Kumar, S. P. Vijayaragavan, and M. Sriram, "Removal of high density salt and pepper noise in color image through modified cascaded filter," *Journal of Ambient Intelligence and Humanized Computing*, vol. 12, no. 3, pp. 3901–3908, 2021, doi: 10.1007/s12652-020-01737-1.
[2] C. Tian, L. Fei, W. Zheng, Y. Xu, W. Zuo, and C. W. Lin, "Deep learning on image denoising: An overview," *Neural Networks*, vol. 131, pp. 251–275, 2020, doi: 10.1016/j.neunet.2020.07.025.
[3] Y. Quan, Y. Chen, Y. Shao, H. Teng, Y. Xu, and H. Ji, "Image denoising using complex-valued deep CNN," *Pattern Recognition*, vol. 111, p. 107639, 2021, doi: 10.1016/j.patcog.2020.107639.
[4] I. Hong, Y. Hwang, and D. Kim, "Efficient deep learning of image denoising using patch complexity local divide and deep conquer," *Pattern Recognition*, vol. 96, 2019, doi: 10.1016/j.patcog.2019.06.011.
[5] S. Rawat, K. P. S. Rana, and V. Kumar, "A novel complex-valued convolutional neural network for medical image denoising," *Biomedical Signal Processing and Control*, vol. 69, no. May, p. 102859, 2021, doi: 10.1016/j.bspc.2021.102859.
[6] B. Garg, "An adaptive minimum-maximum value-based weighted median filter for removing high density salt and pepper noise in medical images," *International Journal of Ad Hoc and Ubiquitous Computing*, vol. 35, no. 2, pp. 96–116, 2020, doi: 10.1504/IJAHUC.2020.109795.
[7] H. Hwang and R. A. Haddad, "Adaptive median filters: new algorithms and results," *IEEE Transactions on Image Processing*, vol. 4, no. 4, pp. 499–502, 1995, doi: 10.1109/83.370679.
[8] V. Jayaraj and D. Ebenezer, "A new switching-based median filtering scheme and algorithm for removal of high-density salt and pepper noise in images," *Eurasip Journal on Advances in Signal Processing*, vol. 2010, no. 1, 2010, doi: 10.1155/2010/690218.
[9] D. N. H. Thanh, N. H. Hai, V. B. S. Prasath, L. M. Hieu, and J. M. R. S. Tavares, "A two-stage filter for high density salt and pepper denoising," *Multimedia Tools and Applications*, vol. 79, no. 29–30, pp. 21013–21035, 2020, doi: 10.1007/s11042-020-08887-6.
[10] J. Varghese, N. Tairan, and S. Subash, "Adaptive switching non-local filter for the restoration of salt and pepper impulse-corrupted digital images," *Arabian Journal for Science and Engineering*, vol. 40, no. 11, pp. 3233–3246, 2015, doi: 10.1007/s13369-015-1799-2.
[11] U. Erkan, L. Gökrem, and S. Enginoğlu, "Different applied median filter in salt and pepper noise," *Computers and Electrical Engineering*, vol. 70, pp. 789–798, 2018, doi: 10.1016/j.compeleceng.2018.01.019.
[12] M. H. Lee and S. Y. Shin, "Modified pixels based fast median filter in impulse noise environments," *Indonesian Journal of Electrical Engineering and Computer Science*, vol. 9, no. 3, pp. 731–741, 2018, doi: 10.11591/ijeecs.v9.i3.pp731-741.
[13] S. Enginoğlu, U. Erkan, and S. Memiş, "Pixel similarity-based adaptive Riesz mean filter for salt-and-pepper noise removal," *Multimedia Tools and Applications*, vol. 78, no. 24, pp. 35401–35418, 2019, doi: 10.1007/s11042-019-08110-1.
[14] F. Ahmed and S. Das, "Removal of high-density salt-and-pepper noise in images with an iterative adaptive fuzzy filter using alpha-trimmed mean," *IEEE Transactions on Fuzzy Systems*, vol. 22, no. 5, pp. 1352–1358, 2014, doi: 10.1109/TFUZZ.2013.2286634.
[15] M. González-Hidalgo, S. Massanet, A. Mir, and D. Ruiz-Aguilera, "Improving salt and pepper noise removal using a fuzzy mathematical morphology-based filter," *Applied Soft Computing Journal*, vol. 63, pp. 167–180, 2018, doi: 10.1016/j.asoc.2017.11.030.

[16] A. A. Hussein, S. A. Hussain, and A. H. Reja, "Image mixed gaussian and impulse noise elimination based on sparse representation model," *Indonesian Journal of Electrical Engineering and Computer Science*, vol. 23, no. 3, pp. 1440–1450, 2021, doi: 10.11591/ijeecs.v23.i3.pp1440-1450.

[17] M. Azhar, H. Dawood, H. Dawood, G. I. Choudhary, A. K. Bashir, and S. H. Chauhdary, "Detail-preserving switching algorithm for the removal of random-valued impulse noise," *Journal of Ambient Intelligence and Humanized Computing*, vol. 10, no. 10, pp. 3925–3945, 2019, doi: 10.1007/s12652-018-1153-0.

[18] M. Panda, D. P. Mishra, S. M. Patro, and S. R. Salkuti, "Prediction of diabetes disease using machine learning algorithms," *IAES International Journal of Artificial Intelligence*, vol. 11, no. 1, pp. 284–290, 2022, doi: 10.11591/ijai.v11.i1.pp284-290.

[19] J. M. Z. Hoque, J. Hossen, S. Sayeed, K. C. M. Tawsif, J. Ganesan, and J. E. Raja, "Automatic missing value imputation for cleaning phase of diabetic s readmission prediction model," *International Journal of Electrical and Computer Engineering*, vol. 12, no. 2, pp. 2001–2013, 2022, doi: 10.11591/ijece.v12i2.pp2001-2013.

[20] S. Bhutia, B. Patra, and M. Ray, "COVID-19 epidemic: analysis and prediction," *IAES International Journal of Artificial Intelligence*, vol. 11, no. 2, pp. 736–745, 2022, doi: 10.11591/ijai.v11.i2.pp736-745.

[21] P. Jain and V. Tyagi, "LAPB: Locally adaptive patch-based wavelet domain edge-preserving image denoising," *Information Sciences*, vol. 294, pp. 164–181, 2015, doi: 10.1016/j.ins.2014.09.060.

[22] J. R. F. Raj, K. Vijayalakshmi, and S. K. Priya, "Medical image denoising using multi-resolution transforms," *Measurement: Journal of the International Measurement Confederation*, vol. 145, no. January, pp. 769–778, 2019, doi: 10.1016/j.measurement.2019.01.001.

[23] M. A. Aslam, M. A. Munir, and D. Cui, "Noise removal from medical images using hybrid filters of technique," *Journal of Physics: Conference Series*, vol. 1518, no. 1, 2020, doi: 10.1088/1742-6596/1518/1/012061.

[24] G. Jeon, "Computational intelligence approach for medical images by suppressing noise," *Journal of Ambient Intelligence and Humanized Computing*, vol. 0, no. 0, pp. 1–11, 2017, doi: 10.1007/s12652-017-0627-9.

[25] V. Singh, R. Dev, N. K. Dhar, P. Agrawal, and N. K. Verma, "Adaptive Type-2 Fuzzy Approach for Filtering Salt and Pepper Noise in Grayscale Images," *IEEE Transactions on Fuzzy Systems*, vol. 26, no. 5, pp. 3170–3176, 2018, doi: 10.1109/TFUZZ.2018.2805289.

[26] Y. A. Fadil, B. Al-Bander, and H. Y. Radhi, "Enhancement of medical images using fuzzy logic," *Indonesian Journal of Electrical Engineering and Computer Science*, vol. 23, no. 3, pp. 1478–1484, 2021, doi: 10.11591/ijeecs.v23.i3.pp1478-1484.

[27] C. T. Lu, M. Y. Chen, J. H. Shen, L. L. Wang, N. Y. Yen, and C. H. Liu, "X-ray bio-image denoising using directional-weighted-mean filtering and block matching approach," *Journal of Ambient Intelligence and Humanized Computing*, vol. 0, no. 0, pp. 1–18, 2018, doi: 10.1007/s12652-018-0692-8.

[28] P. R. Chanu and K. M. Singh, "Impulse noise removal from medical images by two stage quaternion vector median filter," *Journal of Medical Systems*, vol. 42, no. 10, 2018, doi: 10.1007/s10916-018-1057-8.

[29] N. R. Hamza, R. A. Dihin, and M. H. Abdulameer, "A hybrid image similarity measure based on a new combination of different similarity techniques," *International Journal of Electrical and Computer Engineering*, vol. 10, no. 2, pp. 1814–1822, 2020, doi: 10.11591/ijece.v10i2.pp1814-1822.

[30] N. Asuni and A. Giachetti, "Testimages: A large-scale archive for testing visual devices and basic image processing algorithms," *Italian Chapter Conference 2014 - Smart Tools and Apps in Computer Graphics, STAG 2014*, pp. 63–70, 2014, doi: 10.2312/stag.20141242.

BIOGRAPHIES OF AUTHORS

Shiju Thomas is a research scholar in the department of computer science, school of engineering and technology, Christ university and also working as an assistant professor at the Rajagiri College of Social Sciences. He received his MCA and M Tech degrees in Computer Science from the Cochin University of Science and Technology in 2002 and 2016, respectively. His current research interests include image restoration, steganography, and encryption then compression systems. He can be contacted at email: shijuthomascochin@gmail.com.

Addapalli Krsihna is working as a professor in the department of computer science and engineering, school of engineering and technology, Christ university. He received his BE, ME and M Tech degrees in Cdegreesr Science in the years 1987, 1994, and 2010, respectively. He also holds PhD in the area of encryption from Acharya Nagarjuna University in 2010. He is the author of more than 20 journal papers and has written a few book chapters. He can be contacted at email: adapalli.krishna@christuniversity.in.